Interaction of Low-Energy Ions and Atoms of Light Elements with a Fluorinated Carbon Molecular Lattice

ARTICLE *in* THE JOURNAL OF PHYSICAL CHEMISTRY A · APRIL 2007

Impact Factor: 2.69 · DOI: 10.1021/jp066236s · Source: PubMed

2 AUTHORS, INCLUDING:

Pavel Avramov
Siberian Federal University
92 PUBLICATIONS **522** CITATIONS

Interaction of Low-Energy Ions and Atoms of Light Elements with a Fluorinated Carbon Molecular Lattice

Pavel V. Avramov*,†,‡ and Boris I. Yakobson§

Takasaki-branch, Advanced Science Research Center, Japan Atomic Energy Agency, Takasaki, 370-1292, Japan, L.V. Kirensky Institute of Physics SB RAS, 660036 Krasnoyarsk, Russian Federation, and Department of Mechanical Engineering and Material Science, and Department of Chemistry, Rice University, Houston, Texas 77005

Received: September 22, 2006; In Final Form: December 20, 2006

The mechanism of interaction of low-energy atoms and ions of light elements (H, H^+, He, Li, the kinetic energy of the particles 2−40 eV) with C_6H_6, C_6F_{12}, C_{60}, and $C_{60}F_{48}$ molecules was studied by ab initio MD simulations and quantum-chemical calculations. It was shown that starting from 6 Å from the carbon skeleton for the "C_6H_6 + proton" and "C_{60} + proton" systems, the electronic charge transfer from the aromatic molecule to H^+ occurs with a probability close to 1. The process transforms the H^+ to a hydrogen atom and the neutral C_6H_6 and C_{60} molecules to cation radicals. The mechanism of interaction of low-energy protons with C_6F_{12} and $C_{60}F_{48}$ molecules has a substantially different character and can be considered qualitatively as the interaction between a neutral molecule and a point charge. The Coulomb perturbation of the system arising from the interaction of the uncompensated proton charge with the Mulliken charges of fluorine atoms results in an inversion of the energies of the electronic states localized on the proton and on the C_6F_{12} and $C_{60}F_{48}$ molecules and makes the electronic charge transfer energetically unfavorable. On the different levels of theory, the barriers of the proton penetration for the C_6F_{12} and $C_{60}F_{48}$ molecules are from two to four times lower than those for the corresponding parent systems (C_6H_6 and C_{60}). The penetration barriers of the He atom and Li^+ ion depend mainly on the effective radii of the bombarding particles. The theoretical penetration and escaped barriers for the "Li^+ + C_{60}" process qualitatively explain the experimental conditions of synthesis of the Li@C_{60} complex.

I. Introduction

Development of an effective method of synthesis of endohedral fullerene complexes and nanotubes remains a priority in the chemistry of nanostructures. There are only a few of ways to prepare such nanostructures: (1) high-temperature synthesis in a carbon plasma,[1,2] (2) processing of carbon nanostructures by H_2 and He gases under high pressure,[3,4] (3) irradiation of carbon nanoclusters by low-energy ion beams (30−40 eV),[5,6] and (4) radioactive decay of some elements.[7] Only for the case of irradiation of fullerite by low-energy (30 eV) Li^+ ions the chemical yield of synthesis is about 30%,[6] whereas in all other cases the chemical output is sufficiently lower (0.1−0.01% or less).

The nature of interaction of the guest atoms and molecules with the C_{60} carbon cage determines the possible ways of the synthesis of the endohedral complexes. The low barriers of penetration of the chemical agent (for example, H_2 and He[3,4] or Li^+[5,6]) through the carbon wall make it easy to synthesize the endohedral complexes using fullerite or C_{60} in the gas phase as precursors. Contrary to this, the endohedral complexes with transition metal ions or other chemical agents, the penetration barriers for which are high, can be synthesized only during the high-temperature synthesis from the carbon plasma or as a result of high-energy radioactive decay with really low chemical yield.[1,2,7] To optimize the synthesis conditions of the endohedral complexes with light elements,[3−6] one needs to manipulate the penetration barriers of the species through the carbon wall of the C_{60} molecule. A practical way to achieve the goal is a chemical modification of the C_{60} molecule to decrease the electronic density of active π-states localized perpendicular to the C_6 and C_5 fragments.[8]

Earlier, the potential barrier to the penetration of a proton into a fullerene molecule was calculated by quantum-chemical PRDDO and DFT methods[9] (3.8 eV) as the difference between the total energies of a neutral $C_{60}H$ molecule (hydrogen covalently bonded to one of the carbon atoms on the external side of the C_{60} molecule) and a neutral transition complex where the proton is at the center of a relaxed carbon hexagon. The potential barriers for a He atom have been calculated by the molecular mechanics method (9.4 eV),[10] semiempirical MNDO method[11] (11.5 eV), or using the second-order Möller−Plesset perturbation theory (MP2) with the 6-31G** basis set[12] (10.7 eV for the C_6H_6 molecule).

The main reason for the high penetration barriers for some ions and atoms through a molecular carbon lattice is an active π-electronic system, which tends to form new covalent bonds at the external side of the objects. Hence, the best way to lower this potential barrier could be to neutralize this system by saturation of the carbon−carbon double bonds, for example, by fluorination. At present the most fluorinated derivative of the C_{60} is the $C_{60}F_{48}$ molecule.[13] Previously, the electronic

* Corresponding author. E-mail: avramov.pavel@jaea.go.jp; phone: +81 027 346 9670; fax: +81 027 346 9696.
† Japan Atomic Energy Agency.
‡ L.V. Kirensky Institute of Physics SB RAS.
§ Rice University.

10.1021/jp066236s CCC: $37.00
Published on Web 02/03/2007

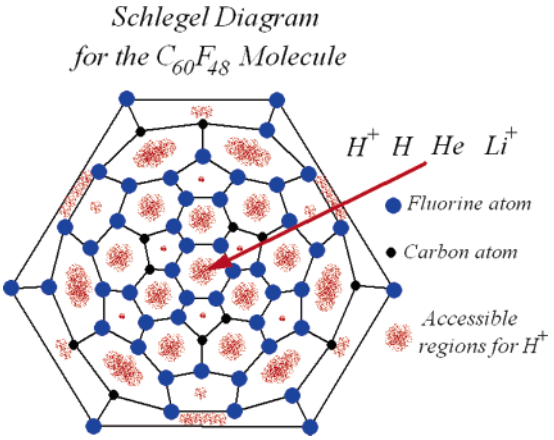

Figure 1. Schlegel diagram for a $C_{60}F_{48}$ molecule. The blue circles denote fluorine atoms, and the black dots represent carbon atoms not connected with fluorine. Red shaded regions reflect regions on the surface of $C_{60}F_{48}$ accessible for low-energy protons.

structure of $C_{60}F_{48}$ has been studied experimentally by photoelectron spectroscopy[13] and theoretically by the ab initio 6-31G method.[14]

II. Atomic and Electronic Structures of $C_{60}F_{48}$ and Details of the Calculations

The $C_{60}F_{48}$ molecule has S_6 symmetry (the Schlegel diagram for the $C_{60}F_{48}$ molecule is presented in Figure 1).[13] There are 3 types of carbon hexagons in the C_{60} atomic lattice: 2 hexagons with 6 fluorine atoms each, 12 hexagons with 5 fluorine atoms, and 6 hexagons with 4 fluorine atoms. There are also two types of carbon pentagons: with five fluorine atoms (six pentagons) and with three fluorine atoms (six pentagons). Single carbon−carbon bonds are divided into four types (the ab initio 6-31G* level): 1.49, 1.54, 1.56, and 1.59 Å. The length of six double carbon−carbon bonds is 1.31 Å, and the length of a fluorine−carbon bond is 1.34 Å.

To study the process of interaction of low-energy (∼10−100 eV) ions and atoms with molecular targets, the kinetic energy of the projectiles should be taken into account. The kinetic energy of the projectiles to penetrate the carbon cage even for light elements (H^+, H, He, Li^+, which can be characterized by small effective radii) is sufficiently higher the energy of molecular vibrations (∼0.1 eV). Even for the low-energy collisions, the effective speed of the projectiles is sufficiently higher (∼2−10 times) than the effective speed of molecular vibrations of the atoms composing a molecule. The process of interaction the low-energy particles should generate a number of vibrational modes of the target molecules with additional dissipation of the projectile energy. The modes (and consequently the amount of dissipated energy) can and should be different for different trajectories and initial collision energies.

The electronic structure calculations of the specific points (global and local minima and transitional states) cannot take into account these features of the collision processes and, from a general point of view, cannot be directly applied to calculate the true potential barriers of the projectile penetration through the carbon cage of the C_{60} and its derivatives. Moreover, because of the large difference in the effective speed of the projectiles and vibration movements of the atoms composing a molecule, an achievement of a number of specific points on the molecular potential energy surface is not evident and should be clarified using a combination of quantum-chemical and molecular-dynamics calculations.

TABLE 1: Theoretical (Calculated Using the Coopmans Theorem) and Experimental Ionization Potentials of H, He, Li, C_{60}, and $C_{60}F_{48}$ (in Electronvolts)

object	ab initio UHF PM3 (eV)	ab initio UHF 6-31G* (eV)	experiment (eV)
H	13.1	13.6	13.6
He,1st IP		24.87	24.56 [18]
He, 2nd IP		54.42	54.25 [18]
Li	5.30	5.33	5.39 [18]
C_{60}	9.5	7.6	7.6 [17]
$C_{60}F_{48}$	14.2	13.8	12.3 [13]

The mechanisms of the interaction of low-energy protons, helium atom and Li^+ ion (the kinetic energy of the particles is in the range of 2−40 eV) with aromatic C_6H_6 and C_{60} molecules (carbon nanostructures (CNS)) and fluorine derivatives C_6F_{12} and $C_{60}F_{48}$ (fluorinated carbon nanostructures (FCNS)) were also investigated using the unrestricted semiempirical UHF PM3 and ab initio 6-31G* quantum-chemical methods using the Gaussian code[15] and molecular-dynamics simulations as well. The optimization of the geometry was performed by the analytical gradient method. All potential barriers were calculated taking into account the basic set superposition error (BSSE). The potential curves for the interaction of a proton with optimized CNS and FCNS were calculated as functions of the distance between the proton and the center of the carbon hexagon lying strictly normal to the direction of motion of the H^+ ion. The penetration of low-energy protons and Li^+ ions through carbon hexagons and pentagons was simulated by the molecular-dynamics method using the UHF PM3 (MD/PM3) and ab initio 6-31G* (MD/6-31G*) potentials.

The applicability of one-determinant wave functions to the description of the electronic structure of fullerenes and their derivatives was confirmed earlier in the work of ref 16. An analysis of the UHF wave function for all different proton positions with respect to the $C_{60}F_{48}$ molecule has shown that the spin contamination of the wave function vanishes in a wide range of distances (0−5 Å). At chemically significant distances from the proton to the center of the carbon hexagon (from 0 to 6 Å), the energy difference between the HOMO and LUMO levels of the "C_{60} + proton", "$C_{60}F_{48}$ + proton", "C_6H_6 + proton", and "C_6F_{12} + proton" systems varied from 5 to 8 eV (depending on the method, system, and distance); this might also argue for the applicability of one-determinant wave functions to the description of such processes. The same difference for the C_{60} + Li^+ and $C_{60}F_{48}$ + Li^+ is sufficiently higher (∼10 eV). It should be noted that because of the presence of a uncompensated positive charge in the systems under study the occupied electron levels are displaced to lower energies to a much greater degree than the unoccupied ones and the number of electrons is always even (according to the condition of the problem). Calculations show that in all cases the electronic states are actually doubly occupied (because the orbitals with spin up and spin down in the UHF method have close energies and have the same character of spatial distribution) and, therefore, the electronic shells are closed.

The unrestricted Hartree−Fock method was chosen for the description of the electronic structure of such dynamic systems because the restricted Hartree−Fock method (RHF, or ROHF in the case of open electronic shells) and various versions of the DFT method incorrectly describe the self-interaction of the hydrogen 1s electron (in these methods, the hydrogen 1s eigenvalues are ca. −6 to 8 eV, whereas the experimental and theoretical (UHF) values of the ionization potential are equal to approximately 13.5 eV; Table 1). This feature of the RHF

and DFT methods does not allow one to correctly describe the initial electronic state of the C_6F_{12} + proton and $C_{60}F_{48}$ + proton systems at infinity, which is formally excited: the hydrogen 1s state with an energy of about −13.5 eV is vacant, and the HOMO level in CNS/FCNS with an energy higher than −12 eV is occupied.

a. Interaction of the Low-Energy Protons with CNS and FCNS. To illustrate the results of direct MD simulations of the "H^+ + CNS/FCNS" interactions, let us develop a simplified perturbation model of the collision process. In the most complex case, the initial state of the "carbon nanostructure plus proton" system (proton−target distance $R_H = -\infty$) is unstable and excited: the low-energy proton at infinity and the neutral molecule as a target (Figure 2). Because of the substantial energy difference (6 eV for the proton + CNS system and 1.3 eV for the proton + FCNS system; Table 1), an electron transition should occur from the occupied electronic states of the carbon nanoparticle to the unoccupied 1s state of the positive hydrogen ion (which is essentially a proton) as the proton approaches the carbon nanostructure sufficiently closely. For the systems H^+ + CNS and H^+ + FCNS (with the proton moving along the Z axis to the center of the carbon hexagon bonded to the six fluorine atoms and oriented normal to the direction of the proton motion), we can write (in the first order of perturbation theory)

$$H = H_0^{\mathrm{H}} + H_0^{\mathrm{CN}} + V_{\mathrm{e}}(R_{\mathrm{H}}) - \frac{\nabla_{\mathrm{p}}^2(R_{\mathrm{H}})}{2m_{\mathrm{p}}} + V_{\mathrm{N}}(R_{\mathrm{H}}) \qquad (1)$$

Here, H_0^{H} and H_0^{CN} are the Hamiltonians of the unperturbed electronic systems of the proton (having an unoccupied 1s orbit) and of the carbon nanostructure and R_H is the radius vector of the proton, which is parallel to the proton velocity and whose length $|R_H| = t\sqrt{2E_K^p/m_p}$ is equal to the distance between the proton and the center of the carbon hexagon. The time t changes from $-\infty$ to 0; $-\nabla_p^2(R_H)/(2m_p)$ is the operator of the proton kinetic energy; E_K^p is the proton kinetic energy (∼10 eV in our case); and $V_e(R_H)$ and $V_N(R_H)$ are the operators of the Coulomb perturbation for the electronic and nuclear subsystems, respectively, describing the interaction of the uncompensated charge of the proton (H^+) with the Mulliken charges of the atoms of CNS or FCNS.

Modern ab initio molecular dynamics[19] describes the motion of nuclei only for the Born−Oppenheimer potential surfaces, for which one can write the relationship $\sqrt{2E_K^p/m_p} \ll \sqrt{2E_K^e/m_e}$, where E_K^e is the electron kinetic energy and m_p and m_e are the proton and electron masses, respectively. Taking into account the relationship between the masses $m_p/m_e \cong 2 \times 10^3$ and the average kinetic energy of the valence electrons ($E_K^e \sim 1/10$ eV), this approximation can be applied to the description of the interaction of low-energy protons with matter if the proton kinetic energy is not higher than $E_K^p \sim 10^2/10^3$ eV. In our case, $E_K^p \sim 10$ eV.

If the kinetic energy is below this limit, then we can separate the electronic and nuclear parts of eq 1. For the electronic part, in the first order of perturbation theory we can write

$$\epsilon'_{\mathrm{H}}(R_{\mathrm{H}}) = \epsilon^0_{\mathrm{H}} + \Delta\epsilon_{\mathrm{H}}(R_{\mathrm{H}}) \qquad (2)$$

$$\epsilon'_{\mathrm{CN}}(R_{\mathrm{H}}) = \epsilon^0_{\mathrm{CN}} + \Delta\epsilon_{\mathrm{CN}}(R_{\mathrm{H}}) \qquad (3)$$

where $\epsilon'_H(R_H)$ and $\epsilon'_{CN}(R_H)$ are the excited electron energy eigenvalues corresponding to the unperturbed value ϵ_H^0 (the energy of the hydrogen 1s level) and to the unperturbed value

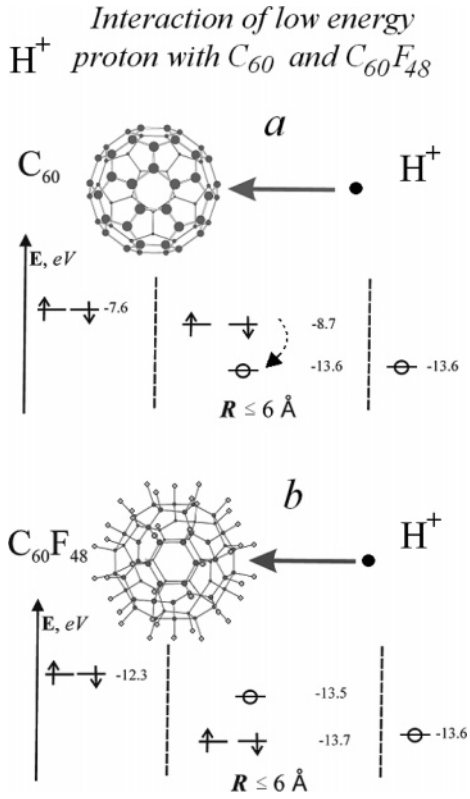

Figure 2. Schematic representation of the interaction of a low-energy proton with (a) C_{60} and (b) $C_{60}F_{48}$ molecules. On the right, the unperturbed eigenvalue of the hydrogen ls orbital (ϵ_H^0) and, on the left, the unperturbed eigenvalue of the carbon nanoparticle (ϵ_{CN}^0) are shown. At the center, perturbed eigenvalues ϵ'_{CN} and ϵ'_H are shown. Over the distance range 0−6 Å in the case of C_{60} molecules, the W_T (the probability of charge transfer) varies from 0 to 1. Because of the charge transfer, the C_{60} molecule becomes a cation radical with the singly occupied $\varphi'_{CN}(\mathbf{r}_{CN})$ state and the proton becomes a hydrogen atom with the singly occupied $\varphi'_H(\mathbf{r}_H)$ state. In the case of the $C_{60}F_{48}$ molecule, charge transfer is suppressed due to the condition $\epsilon'_{CN} < \epsilon'_H$.

ϵ_{CN}^0 (the HOMO level of CNS/FCNS) localized on the proton and on the carbon nanocluster, respectively. For C_{60} and $C_{60}F_{48}$, we have $\epsilon_{CN}^0 = -I_{CN}^E = -7.6$ eV and $\epsilon_{CNF}^0 = -I_{CNF}^E = -12.3$ eV, respectively (where the I_{CN}^E are the experimental ionization potentials,[20,13] see Table 1).

Qualitatively, we can interpret the interaction of a low-energy proton with carbon (fluorine−carbon) nanoclusters in terms of perturbation theory. Disregarding the effects of orbital overlap, we can write the perturbation operator of the electronic system as

$$V_{\mathrm{e}}(R_{\mathrm{H}}) = V^{\mathrm{H}}(\mathbf{r}_{\mathrm{H}}) + V^{\mathrm{C}}(\mathbf{r}_{\mathrm{C}}) + V^{\mathrm{F}}(\mathbf{r}_{\mathrm{F}}) \qquad (4)$$

where $\mathbf{r}_H$, $\mathbf{r}_C$, and $\mathbf{r}_F$ are the radius vectors of the electronic wave functions belonging to the hydrogen, carbon, and fluorine ions, respectively; $V^H(\mathbf{r}_H) = -\sum_i^{N_C} (q_C)/(|\mathbf{r}_H - R_C^i|) + \sum_j^{N_F} (q_F)/(|\mathbf{r}_H - R_F^j|)$ operates only on the $\mathbf{r}_H$ coordinate of the electron wave function (N_C and N_F are the numbers of carbon and fluorine atoms in the system, respectively; $V^C(\mathbf{r}_C) = -\sum_{i=1}^{N_C} (1)/(|\mathbf{r}_C^i + R_C^i|)$ operates on the $\mathbf{r}_C$ coordinate; and $V^F(\mathbf{r}_F) = -\sum_{j=1}^{N_F} (1)/(|\mathbf{r}_F^j + R_F^j|)$ operates on the $\mathbf{r}_F$ coordinate. The vectors R_C^i and R_F^j are directed from the proton to the carbon and fluorine atoms, respectively, and their lengths (for the nearest six neighbors) are $|R_C^i| = \sqrt{R_H^2 + A^2}$ and $|R_F^j| =$

$\sqrt{(R_H-B)^2+C^2}$. The geometrical parameters $A = 1.4$ Å, $B = 1.1$ Å, and $C = 2.4$ Å are determined by the features of the atomic structure of the object; q_C and q_F are the Mulliken charges of the carbon (q_C is zero for C_6H_6 and C_{60} and is equal to ~0.1 for C_6F_{12} and $C_{60}F_{48}$) and fluorine ($q_F \sim -0.1$) atoms.

The interaction $V_N(R_H)$ between the uncompensated proton charge and the Mulliken charges of the atoms of the target molecule also contributes to the energy of the system. For nonfluorinated structures, we have$V_N(R_H) = 0$ because the carbon Mulliken charges are equal to zero. For fluorinated molecules ($C_{60}F_{48}$, C_6F_{12}), the quantity $V_N(R_H) = \sum_i^{N_C} (q_C)/(|R_C^i|) - \sum_j^{N_F} (q_F)/(|R_F^j|)$ describes the contribution to the energy due to the interaction of the Mulliken charges of the carbon and fluorine atoms with the uncompensated charge.

The electronic structure of the system in the initial state of the process (neutral target molecule + proton at infinity) is quasi-excited (the energy of the unoccupied H1s state is −13.6 eV, and the energy of the HOMO level of the target molecule is higher than −12 eV; Table 1). As the proton approaches the target molecule, this excited state must decay with the emission of a photon and charge transfer via the electron transition from the target molecule to the proton. The probability of one-electron dipole transition from the occupied orbital $\varphi_{CN}(\mathbf{r}_{CN})$ localized at the CNS/FCNS to the $\varphi_H(\mathbf{r}_H)$ orbital (the unoccupied hydrogen 1s state) can be written as[20]

$$w_T = 2|L_T|^2/(\hbar\omega)^2 \quad (5)$$

where $L_T = \langle\varphi'_{CN}(\mathbf{r}_{CN})|\mathbf{r}|\varphi'_H(\mathbf{r}_H)\rangle$, $\mathbf{r}$ is the dipole transition operator, and the transition energy is $\hbar\omega = \epsilon'_{CN}(R_H) - \epsilon'_H(R_H)$. The matrix element $L_T \neq 0$ if the overlap integrals for this system $S_{H-CN} = \langle\varphi_H|\varphi_{CN}\rangle \neq 0$ and $|R_H| > 0$ (this condition is satisfied if the system has no mirror symmetry. This is the case for a substantial (of about 1 au) separation between the proton and the center of the carbon hexagon). At large R_H distances (Figure 2), the overlap integrals vanish to zero. Our ab initio UHF/6-31G* calculations show that starting from a distance of ~6 Å from the center of the carbon hexagon ($R_C < 6.3$Å, $R_F < 5.8$Å), the overlap integrals vary from 0 to 0.5. In this interval, $r(R_{CN})$ is equal to several angstroms; therefore, $w_T \approx S_{H-CN}$. The energy differences obtained by the PM3 method show that, in the case of $C_{60}F_{48}$, at a distance of 6 Å, we have $\Delta\epsilon_H = 0.1$ eV and $\Delta\epsilon_{CNF} = -1.4$ eV (the new $\epsilon'_H = -13.5$ and $\epsilon'_{CNF} = -13.7$ eV values were obtained using the theoretical energy shifts and correspondent experimental ionization potentials, Table 1). Thus, at distances of ≤6 Å, the "$C_{60}F_{48}$ + proton" configuration becomes the ground state of the system and the fluorinated carbon nanostructure interacts with a proton as does a neutral molecule with a point charge.

For a low-energy proton (~2 eV), the transit time for a distance of 6 Å is $T = 5 \times 10^{-14}$ s (for the "C_{60} + proton" system with $R_H < 6$ Å, the number of periods of the electronic transition from the occupied state $\varphi_{CN}(\mathbf{r}_{CN})$ to the unoccupied state $\varphi_H(\mathbf{r}_H)$ (Figure 2) is 10^2-10^3). For C_{60}, we have $\Delta\epsilon_H = 0.0$ eV (the Mulliken charge of the carbon atoms is zero) and $\Delta\epsilon_{CN} = -1.15$ eV($\epsilon'_H = -13.6$ eV, $\epsilon'_{CN} = -8.7$ eV). In this case, the transition frequency ω is 10^{16} s^{-1}; therefore, the total transition probability from the molecular level into the unoccupied H1s state (with regard for the number of periods of the electronic transition) is close to 1. The lifetime of the excited electronic state ($\tau \sim (5 \times 10^{-15})/(3 \times 10^{-15})$ s) can be estimated from the experimental width of the photoelectron spectra (0.2−0.3 eV for C_{60}[21,22] and $C_{60}F_{48}$[13]). This lifetime is an order of magnitude shorter than the proton transit time of the distance of 6 Å at which the overlap integral between the wave functions of the carbon nanoparticle and the proton becomes nonzero. On the basis of these estimations, we may assert that the aromatic systems like C_{60} and C_6H_6 interact with a low-energy proton as do positive ion radicals (C_{60}^{+1} and $C_6H_6^{+1}$) with a radical (neutral hydrogen atom). This will certainly facilitate the formation of a new covalent carbon−hydrogen bond on the external side of the carbon nanoparticle.

Both theoretical quantum-chemical methods (UHF PM3 and ab initio UHF/6-31G*) correctly describe the initial "FCNS + proton" state because the first ionization potential of $C_{60}F_{48}$ is overestimated (Table 1) and, therefore, the H1s state in the $C_{60}F_{48}$ + proton system remains unoccupied and all $C_{60}F_{48}$ levels are occupied. This feature allowed us to perform molecular-dynamics simulation of the interaction of protons with FCNS (C_6F_{12} and $C_{60}F_{48}$) using both the semiempirical and ab initio quantum-chemical potentials. For comparison, we performed a molecular-dynamics simulation of the interaction of protons with aromatic carbon molecules (C_{60}, C_6H_6) with one difference: to avoid an error in describing the initial state (neutral molecule + proton at infinity), the initial distance between the proton and the carbon nanoparticle was chosen to be 2 Å. Thus, we assumed that, at this distance, the electron from the carbon nanoparticle has already passed to the proton with the formation of a hydrogen atom. We used the MD/PM3 and MD/UHF 6-31G* methods to simulate the interaction of a proton with C_6H_6 and C_6F_{12} and only the MD/PM3 method to simulate the interaction with C_{60} and $C_{60}F_{48}$ molecules.

b. Interaction of Helium with CNS and FCNS. It is well known that helium has really high first (24.56 eV experiment and 24.87 eV ab initio RHF/6-31G*) and second (54.25 and 54.42 eV respectively) ionization potentials (Table 1). Because of this, the He^+ and He^{2+} (α particle) ions are really strong oxidizers, and both CNS and FCNS systems should interact with low-energy He^+ and He^{2+} as positively charged radicals with neutral helium atoms. Because of this, here we studied only the interactions of the helium atom with CNS and FCNS objects.

c. Interaction of the Low-Energy Lithium Ions with CNS and FCNS. In contrast with helium, lithium has a really small ionization potential (5.39 eV experiment, 5.30 eV UHF PM3 and 5.33 eV ab initio UHF/6-31G*, Table 1). Taking into account the ionization potentials of both types of objects (CNS and FCNS, Table 1), the probability of the charge transfer from the targets (CNS and FCNS) to the Li^+ ions can be estimated close to 0. Evidently, in this situation the quantum-chemical methods can describe correctly the initial state of the process (neutral target molecule and low-energy positive ion on infinity). Because of this, we have performed the ab initio MD/PM3 simulations of interactions of Li^+ with CNS and FCNS in the same way as for the H^+ + FCNS (see the above paragraph).

III. Results and Discussion

The potential curves for the interaction of a proton with $C_{60}F_{48}$ and C_{60} molecules calculated by the UHF PM3 and ab initio UHF/6-31G* methods are shown in Figure 3. The distance R_H was measured from the proton to the center of the carbon hexagon (completely fluorinated in the case of $C_{60}F_{48}$) lying on the trajectory of the approaching proton. The solid and dashed lines represent the results obtained by the ab initio UHF/6-31G* method for the $C_{60}F_{48}$ and C_{60} molecules correspondingly, whereas the solid squares and dots correspond to the UHF PM3 method. The filled upward and downward triangles (the ab initio UHF/6-31G* method) and the open upward and downward ones (the UHF PM3 method) at infinity ($R = -\infty$) denote the total

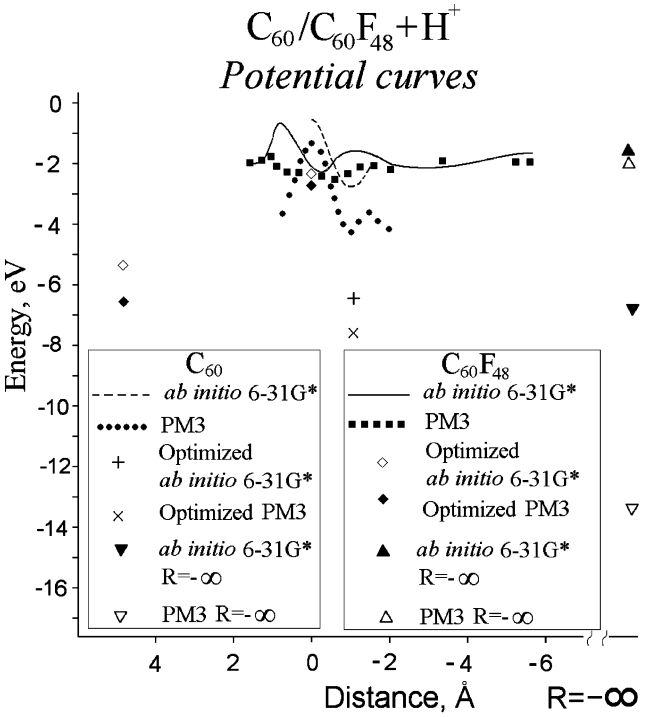

Figure 3. Potential energy curves for the $C_{60}F_{48} + H^+$ and $C_{60} + H^+$ systems. Solid and dashed lines represent the ab initio UHF/6-31G* calculations for $C_{60}F_{48}$ and C_{60} cases, respectively. The solid squares and dots correspond to UHF PM3 calculations. Solid triangles (ab initio UHF/6-31G*, upward for the $C_{60}F_{48}$ and downward for the C_{60}) and open triangles (UHF PM3, upward for the $C_{60}F_{48}$ and downward for the C_{60}) at a distance $R = -\infty$ denote the total energies of the free molecules in the gas phase. The solid (ab initio UHF/6-31G*) and open (UHF PM3) diamonds represent the total energies of the optimized $H-C_{60}F_{48}^+$ structures (with a hydrogen at the center of the carbon hexagon ($R = 0$) or with a covalently bonded hydrogen inside the carbon polyhedron ($R = 5$ Å)), whereas the cross (+) and X character represent the $H-C_{60}^+$ complex with a covalently bonded hydrogen on the external side of the C_{60} molecule ($R = -1$ Å) on the ab initio UHF/6-31G* and UHF/PM3 levels of theory, respectively.

energy of the neutral $C_{60}F_{48}$ and C_{60} molecules in the gas phase. Solid (the ab initio UHF/6-31G* method) and open (UHF PM3 method) dimonds denote the total energy of the optimized $H-C_{60}F_{48}^+$ complexes with the hydrogen placed at the center of the carbon hexagon, $R = 0$, and the hydrogen covalently bonded to an sp^2 carbon inside the carbon polyhedron, $R = 5$ Å. The cross (+) (the ab initio UHF/6-31G*) and X character (UHF PM3) denote the optimized structure of the $H-C_{60}^+$ complex with the hydrogen covalently bonded to an sp^2 carbon outside the C_{60} molecule, $R = -1$ Å.

For the $C_{60}F_{48} + H^+$ system, the potential curves are typically smooth and do not exhibit high potential barriers or wells outside the carbon nanostructure or at the wall. For the $C_{60} + H^+$ system, two deep potential wells outside the carbon nanostructure, corresponding to the initial state (a neutral C_{60} molecule, $R = -\infty$) and to the hydrogen covalently bonded to a carbon atom ($R = -1$ Å), and one high potential barrier at the center of the carbon hexagon ($R = 0$) exist. For the $C_{60}F_{48} + H^+$ system, a deep potential well exists inside the carbon polyhedron ($R = 5$ Å), corresponding to the hydrogen covalently bonded to an sp^2 carbon atom. This bond forms when the incident proton passes through the center of the carbon hexagon and collides with a nonfluorinated carbon atom located on the opposite side of the molecule.

The potential barriers to the penetration of the proton were calculated as the difference between the energies of the intermediate state (a guest atom at the center of the carbon hexagon) and of the initial state (the proton covalently bonded to a carbon atom on the external side of the carbon polyhedron[9]) or as the difference between the energies of the intermediate state and a neutral state of the C_{60} molecule. The choice of the former initial state of the process of proton penetration through the carbon polyhedron is related not only to compare our data with the results of the work of ref 9 but also to the obvious fact that this configuration corresponds to the global energy minimum of the system, to which the system will tend in the case where the proton kinetic energy is close to zero.

TABLE 2: Potential Barriers and Kinetic Energies Required for a Proton to Penetrate through the Center of a Carbon Hexagon (Results of Ab Initio UHF/6-31G* Calculations)

object	potential barrier (eV)	kinetic energy (eV)
$C_6H_6 + H^+$	5.6	6.7
$C_6F_{12} + H^+$	1.4	2.6
$C_{60} + H^+$	6.2 (6.3)[a]	
$C_{60}F_{48} + H^+$	3.1	
$C_{60} + He$	14.0	
$C_{60}F_{48} + He$	10.5	

[a] Note: The potential barrier was calculated as the difference between the energies of the intermediate state (with a proton at the center of the hexagon) and of the free C_{60} molecule is indicated in parentheses. The calculations were performed taking into account the BSSE error.

TABLE 3: Potential Barriers and the Kinetic Energies Required for a Proton to Penetrate through Carbon Hexagons (Results of the UHF PM3 Calculations)

object	potential barrier (eV)	kinetic energy (eV)
$C_6H_6 + H^+$	6.5	5.6
$C_6F_{12} + H^+$	4.8	3.7
$C_{60} + H^+$	6.5 (12.0)[a]	5.7
$C_{60}F_{48} + H^+$	1.8	1.4
$C_{60} + Li^+$		18.6
$C_{60}F_{48} + Li^+$		17.6

[a] The meaning of the parenthetical value is explained in the footnote of Table 2.

Using molecular dynamics, we calculated the kinetic energy of the penetration of a proton or Li^+ ion as the minimum kinetic energy required for the particle to penetrate into the molecule through the center of the carbon hexagon. In the case of the $C_{60}F_{48}$ molecule, the center of the completely fluorinated carbon hexagon was chosen as a target. The calculated penetration barriers are listed in Tables 2 and 3 (ab initio UHF/6-31G* and UHF PM3 methods, respectively).

The ab initio UHF/6-31G* calculations (Table 2) show a significantly lower barrier (by up to four times in the case of C_6H_6/C_6F_{12} molecules) for the penetration of a proton through the carbon hexagon of FCNS (C_6F_{12} and $C_{60}F_{48}$) as compared to the barriers of nonfluorinated C_{60} and C_6H_6 molecules. We explain this result in terms of a substantial decrease in the density of valence π-electrons on fluorinated nanoobjects, which precludes the formation of new covalent hydrogen−carbon bonds on the external side of the carbon polyhedron. Nevertheless, the potential barrier to the escape of the proton from the $C_{60}F_{48}$ molecule remains high (~5 eV) because of the formation of a new carbon−hydrogen covalent bond inside the carbon nanostructure (Figure 3).

The potential barrier for a helium atom is 25% lower for fluorinated nanostructures as compared to nonfluorinated nano-

TABLE 4: Ionic and Atomic Radii of the Light Elements[18]

element	atomic radius (Å)	ionic radius (Å)
H (H^+)	0.79	0.012
He	0.49	
Li (Li^+)	2.05	0.76

structures (Table 2); this fact can be explained by the 12.5% lengthening of the carbon−carbon distance in a $C_{60}F_{48}$ molecule (1.59 Å) as compared to that in a C_{60} molecule (1.40 Å) and by the decrease in the density of π clouds at the center of the carbon hexagon.

For C_6H_6 and C_6F_{12} molecules, we performed the molecular-dynamics simulation using the ab initio UHF/6-31G* potential (MD/6-31G*). The proton kinetic energy at which the H^+ penetrates through the C_6 fragment turned out to be 2.6 times lower for a C_6F_{12} molecule (2.6 eV) than that for a benzene molecule (6.7 eV; Table 2). We did not study the potential curves for the interaction of a proton with a C_6F_{12} molecule because of the substantial distortion of the C_6 fragment in this case and the impossibility of defining its center uniquely.

Similar results for the $C_6H_6 + H^+$ and $C_6F_{12} + H^+$ systems were also obtained by the semiempirical PM3 method (Table 3). The potential barrier for a $C_{60}F_{48}$ molecule (1.8 eV) turned out to be 3.6 times lower than that for a C_{60} molecule (6.5 eV). This ratio for the pair C_6F_{12} (4.8 eV) and C_6H_6 (6.5 eV) is much lower (∼1.4) because the PM3 method predicts that the C−C bond in the C_6F_{12} molecule can be broken by the proton. Simulation of the $(C_{60} + H^+)/(C_{60}F_{48} + H^+)$ and $(C_6H_6 + H^+)/(C_6F_{12} + H^+)$ processes using the MD/PM3 method showed that fluorination lowers the penetration barriers by factors of 4.1 and 1.5, respectively. It should be noted that after the penetration into the carbon polyhedron of the $C_{60}F_{48}$ molecule the proton forms a new C−H bond with an sp^2 carbon atom inside the carbon skeleton. Subsequent collisions with protons form either new carbon−hydrogen bonds inside the $C_{60}F_{48}$ molecule or H_2 molecules via the breaking of the earlier formed carbon−hydrogen bonds.

The MD/PM3 simulations of the processes $C_{60} + Li^+$ and $C_{60}F_{48} + Li^+$ (Table 3) show that there is no significant difference between penetration barriers for the $C_{60}F_{48}$ (17.6 eV) and C_{60} (18.6 eV). The Li^+ ion is chemically passive in both cases because of low ionization potential. The escape barrier for both molecules remains high and practically the same (the initial kinetic energy of the ions is 31.4 and 32.3 eV for $C_{60}F_{48}$ and C_{60}, respectively). The high value of the escape barrier can explain quantitatively the experimental data of E.E.E. Campbell[6] described shortly in the introduction. According to this data, the endohedral complexes of the C_{60} can be created using Li^+ ion beams with the kinetic energy around 30 eV. The consequent increasing of the kinetic energy of the Li^+ ions during our MD simulations leads to a destroying of the carbon cage of the C_{60}/$C_{60}F_{48}$ and escape of the Li^+ ions from both molecules.

Collisions of the low-energy He and Li^+ with C_{60} and $C_{60}F_{48}$ as well as the $H^+ + C_{60}F_{48}$ ones can be rated as the interactions of chemically passive particles with neutral molecules. Increasing of the potential barriers in the line H^+, He, and Li^+ can be explained by increasing of the ionic/atomic radii of the species (Table 4).

We also studied other channels of inelastic scattering of protons by a $C_{60}F_{48}$ molecule using the MD/PM3 method. As a target, we chose (i) a carbon atom not bonded to a fluorine atom, (ii) the center of the double carbon−carbon bond, (iii) the center of the carbon pentagon, (iv) a fluorine atom, (v) the center of the carbon−fluorine bond, and (vi) a series of points on an imaginary surface of carbon pentagons and hexagons lying far from their centers.

Molecular-dynamics simulation showed that there are several channels of inelastic scattering of protons with a kinetic energy of about 2 eV:

(1) Breaking of a C−F bond with the formation of a HF molecule (collisions with a carbon atom, with the centers of the carbon−carbon and carbon−fluorine bonds).

(2) Penetration into a $C_{60}F_{48}$ molecule (through a number of points on the imaginary surface of carbon pentagons and hexagons).

(3) Reflection of the proton with partial absorption of its kinetic energy via the excitation of molecular vibrations of the $C_{60}F_{48}$ molecule (in particular, due to collisions with fluorine atoms).

The same trajectories were also studied for the $Li^+ + C_{60}F_{48}$ collisions with kinetic energy close to 30 eV. The MD simulations also demonstrate some alternative channels of inelastic scattering of the Li^+ ions with breaking the C−F bonds and consiquent formation of the LiF molecules or breaking the C_{60} cage itself.

The results of the MD/PM3 calculations showed that, on the imaginary surface of carbon hexagons in $C_{60}F_{48}$, there are regions with a reduced electronic density that are open for proton penetration. For example, for a kinetic energy of 2 eV, the diameter of such a region is ∼1.5 Å. Therefore, approximately 25% of the imaginary surface of the carbon polyhedron of fluorinated nanoobjects is open for proton penetration through the walls. The schematic representation of the accessible proton areas are presented in Figure 1 by shaded red regions.

VI. Conclusions

In this study we have shown that starting from a distance of ∼6 Å the electronic charge transfer determines the character of interaction of low-energy protons with aromatic molecules and transforms a proton into a hydrogen atom and a neutral target molecule into a cation radical. In turn, this circumstance facilitates the formation of a new covalent carbon−hydrogen bond outside the carbon nanoparticle and determines the nature of the potential barrier to the penetration of a proton through carbon pentagons and hexagons.

The presence of substitutional fluorine atoms suppresses the electronic charge transfer from C_6F_{12} and $C_{60}F_{48}$ due to the Coulomb perturbation of the electronic structure of an interacting system. In this case, the neutral $C_6F_{12}/C_{60}F_{48}$ molecule + proton state becomes the ground state and, therefore, the low-energy proton interacts with fluorinated carbon nanoparticles as a point charge does with a neutral molecule. At short (chemically significant) distances of ∼2 Å, the absence of the π-electron density on the external side of the carbon polyhedron precludes the formation of a new C−H bond. In turn, this lowers the barriers to the penetration of low-energy protons through the carbon cage by a factor of 2−4.

Molecular-dynamics simulations using the ab initio UHF 6-31G* and semiempirical potentials have shown that, for a proton kinetic energy of 2 eV, a quarter of the imaginary surface of the carbon cage of the fluorine-substituted carbon molecules is open for the penetration of low-energy protons. However, the barrier to the escape of a proton from such molecules remains high because of the formation of new covalent carbon−hydrogen bonds inside the systems under study. Other scattering channels result either in the carbon−fluorine bond breaking (with the formation of HF molecules) or in the reflection of a

proton from the molecules with a loss of part of the kinetic energy due to the excitation of molecular vibrations in the fluorine−carbon nanoparticle.

The He atoms and Li^+ ions are chemically passive for both types of molecules, and the barrier heights depend only on the effective radii of the bombardment particles.

Acknowledgment. Work at Rice University was supported by the Office of Naval Research, by the Robert Welch Foundation, and by the Nanoscale Science and Engineering Initiative of the National Science Foundation (CBEN). Research at ASRC was supported by JAERI/JAEA project "Materials Design with New Functions Employing Energetic Beams" and JAERI/JAEA Research fellowship (P.V.A.). P.V.A. also thanks Prof. Yoshihito Maeda and the personnel of JAERI/JAEA Research Group for Atomic-scale Control for Novel Materials under Extreme Conditions for hospitality and fruitful discussions.

References and Notes

(1) Heath, J. R.; O'Brien, S. C.; Zhang, Q.; Liu, Y.; Curl, R. F.; Kroto, H. W.; Tittel, F. K.; Smalley, R. E. *J. Am. Chem. Soc.* **1985**, *107*, 7779.

(2) Chai, Y.; Guo, T.; Jin, C.; Haufler, R. E.; Chibante, L. P. F.; Fure, J.; Wang, L.; Alford, J. M.; Smalley, R. E. *J. Phys. Chem.* **1991**, *95*, 7564.

(3) Saunders, M.; Jimenez-Vazquez, H. A.; Cross, R. J.; Poreda, R. J. *Science* **1993**, *259*, 1428.

(4) Christian, J. J.; Wan, Z.; Anderson, S. L. *Chem. Phys. Lett.* **1992**, *199*, 373.

(5) Murphy, T. A.; Pawlik, T.; Weidinger, A.; Höhne, M.; Alcala, R.; Spaeth, J. M. *Phys. Rev. Lett.* **1996**, *77*, 1075.

(6) Campbell, E. E. B.; Tellgmann, R.; Krawez, N.; Hertel, I. V. *J. Phys. Chem. Solids* **1997**, *58*, 1763.

(7) Ohtsuki, T.; Ohno, K.; Shiga, K.; Kawazoe, Y.; Maruyama, Y.; Masumoto, K. *Phys. Rev. Lett.* **1998**, *81*, 967.

(8) Yakobson, B. I.; Avramov, P. V.; Margrave, J. L.; Mickelson, E. T.; Hauge, R. H.; Boul, P. J.; Huffman, C. B.; Smalley R. E. High-Yield Method of Endohedrally Encapsulating Species inside Fluorinated Fullerene Nanocages. U.S. Patent 20040258603, December 23, 2004. Class: 42344500B (USPTO), D01F009/12 (Intl Class).

(9) Estreicher, S. K.; Lathan, C. D.; Heiggie, M. I.; Jones, R.; Öberg, S. *Chem. Phys. Lett.* **1992**, *196*, 311.

(10) Mowrey, K. C.; Ross, M. M.; Callahan, J. H. *J. Phys. Chem.* **1992**, *96*, 4755.

(11) Kolb, M.; Thiel, W. *J. Comput. Chem.* **1993**, *14*, 37.

(12) Hruŝak, J.; Böhme, D. K.; Weiske, T.; Schwarz, H. *Chem. Phys. Lett.* **1992**, *193*, 97.

(13) Mitsumoto, R.; Araki, T.; Ito, E.; Ouchi, Y.; Seki, K.; Kikuchi, K.; Achiba, Y.; Kurosaki, H.; Sonoda, T.; Kobayashi, H.; Boltalina, O. V.; Pavlovich, V. K.; Sidorov, L. N.; Hattori, Y.; Liu, N.; Yajima, S.; Kawasaki, S.; Okino, F.; Touhara, H. *J. Phys. Chem. A* **1998**, *102*, 552.

(14) Bulusheva, L. G.; Okotrub, A. V.; Boltalina, O. V. *J. Phys. Chem. A.* **1999**, *103*, 9921.

(15) Frisch, M. J.; Trucks, G. W.; Schlegel, H. B.; Scuseria, G. E.; Robb, M. A.; Cheeseman, J. R.; Montgomery, J. A., Jr.; Vreven, T.; Kudin, K. N.; Burant, J. C.; Millam, J. M.; Iyengar, S. S.; Tomasi, J.; Barone, V.; Mennucci, B.; Cossi, M.; Scalmani, G.; Rega, N.; Petersson, G. A.; Nakatsuji, H.; Hada, M.; Ehara, M.; Toyota, K.; Fukuda, R.; Hasegawa, J.; Ishida, M.; Nakajima, T.; Honda, Y.; Kitao, O.; Nakai, H.; Klene, M.; Li, X.; Knox, J. E.; Hratchian, H. P.; Cross, J. B.; Bakken, V.; Adamo, C.; Jaramillo, J.; Gomperts, R.; Stratmann, R. E.; Yazyev, O.; Austin, A. J.; Cammi, R.; Pomelli, C.; Ochterski, J. W.; Ayala, P. Y.; Morokuma, K.; Voth, G. A.; Salvador, P.; Dannenberg, J. J.; Zakrzewski, V. G.; Dapprich, S.; Daniels, A. D.; Strain, M. C.; Farkas, O.; Malick, D. K.; Rabuck, A. D.; Raghavachari, K.; Foresman, J. B.; Ortiz, J. V.; Cui, Q.; Baboul, A. G.; Clifford, S.; Cioslowski, J.; Stefanov, B. B.; Liu, G.; Liashenko, A.; Piskorz, P.; Komaromi, I.; Martin, R. L.; Fox, D. J.; Keith, T.; Al-Laham, M. A.; Peng, C. Y.; Nanayakkara, A.; Challacombe, M.; Gill, P. M. W.; Johnson, B.; Chen, W.; Wong, M. W.; Gonzalez, C.; Pople, J. A. *Gaussian 03*, revision C.02; Gaussian, Inc.: Wallingford, CT, 2004.

(16) Andreoni, W. *Annu. Rev. Phys. Chem.* **1998**, *49*, 405.

(17) Hedberg, K.; Hedberg, L.; Bethune, D. S.; Brown, C. A.; de Vries, M. S.; Johnson, R. D. *Science* **1991**, *254*, 410.

(18) CRC Handbook of Chemistry and Physics, 85th ed., 2004−2005; CRC Press: Boca Raton, FL.

(19) Car, R.; Parinello, M. *Phys. Rev. Lett.* **1985**, *55*, 2471.

(20) Landau, L. D.; Lifshitz, E. M. *Course of Theoretical Physics*; Pergamon: New York, 1977; Vol. 3.

(21) Weaver, J. H. *Acc. Chem. Res.* **1992**, *25*, 143.

(22) Varganov, S. A.; Avramov, P. V.; Ovchinnikov, S. G. *Phys. Solid State* **2000**, *42*, 2168.